University of Zawia Journal of Engineering Sciences and Technology (UZJEST)
Volume 4, Issue 2, (2026), pp 121-134, ISSN 3006-2764

Vertical Accuracy Assessment of the AW3D30 Digital Surface Model Using GNSS Checkpoints North of Al-Marj, Libya

Sanaa Ali [1], Basim Younus *[1]

[1] Civil Engineering Department, Higher Institute of Science and Technology, Al-Marj, Libya
*Corresponding author email:basimyounus06@gmail.com

Received: 15-07-2026 | Accepted: 22-09-2026 | Available online: 27-09-2026 | DOI:10.26629/uzjest.2026.10

ABSTRACT

Global digital elevation models are widely used, but their vertical performance varies with terrain and geographic setting. This study assessed the vertical accuracy of the ALOS World 3D–30 m digital surface model (AW3D30) north of Al-Marj, northeastern Libya, using 23 Global Navigation Satellite System (GNSS) checkpoints. Both datasets were referenced to a common coordinate system, and orthometric heights were referenced to the Earth Gravitational Model 1996. Vertical differences, computed as AW3D30 minus GNSS elevation, were summarised using mean error, mean absolute error, root mean square error, and sample standard deviation. Inverse distance weighting (IDW) was used for exploratory visualisation of broad spatial variation. AW3D30 was higher at all checkpoints, with differences ranging from 2.19 to 9.78 m. Mean error and mean absolute error were both 7.04 m, while root mean square error and sample standard deviation were 7.44 and 2.45 m, respectively. Larger differences occurred mainly among the higher sampled elevations, although the dataset could not confirm a continuous elevation difference relationship. The IDW surface suggested lower differences in the western and northwestern sectors, but uneven sampling and the absence of independent validation limited interpretation. Uncorrected AW3D30 elevations should therefore be used cautiously in applications requiring vertical accuracy better than the observed local performance.

Keywords: ALOS AW3D30; vertical accuracy; GNSS validation; digital surface model.

تقييم الدقة الرأسية لنموذج السطح الرقمي AW3D30 باستخدام نقاط تحقق GNSS شمال مدينة المرج، ليبيا

سناء علي[1]، باسم يونس[1]

[1] قسم الهندسة المدنية، المعهد العالي للعلوم والتقنية، المرج، ليبيا

ملخـــــــص البحـــــــث

تُستخدم النماذج الرقمية العالمية للارتفاعات على نطاق واسع، إلا أن أداءها الرأسي يختلف باختلاف طبيعة التضاريس والبيئة الجغرافية. هدفت هذه الدراسة إلى تقييم الدقة الرأسية لنموذج السطح الرقمي العالمي **ALOS World 3D** بدقة مكانية اسمية تبلغ 30 م **(AW3D30)** في المنطقة الواقعة شمال مدينة المرج، شمال شرق ليبيا، باستخدام 23 نقطة تحقق مقاسة بنظام الملاحة العالمي بالأقمار الصناعية **(GNSS).** وقد أُسندت مجموعتا البيانات إلى نظام إحداثي موحّد، وإلى ارتفاعات أرثو مترية مرجعة إلى نموذج الجاذبية الأرضية لعام 1996. وحُسبت الفروق الرأسية على أساس طرح ارتفاعات

"Articles published in *Univ Zawia J Eng Sci Technol* are licensed under a Creative Commons Attribution-NonCommercial 4.0 International License."

GNSS من ارتفاعات**AW3D30** ، ثم لُخّصت باستخدام متوسط الخطأ، ومتوسط الخطأ المطلق، والجذر التربيعي لمتوسط مربعات الخطأ، والانحراف المعياري للعينة. كما استُخدمت طريقة الترجيح العكسي للمسافة **(IDW)** لأغراض التمثيل الاستكشافي للتباين المكاني العام. أظهر **AW3D30** ارتفاعات أعلى عند جميع نقاط التحقق، وتراوحت الفروق بين 2.19 و9.78 م. وبلغ كل من متوسط الخطأ ومتوسط الخطأ المطلق 7.04 م، في حين بلغ الجذر التربيعي لمتوسط مربعات الخطأ والانحراف المعياري للعينة 7.44 و2.45 م على التوالي. وظهرت الفروق الأكبر أساساً عند الارتفاعات الأعلى ضمن العينة، إلا أن البيانات لم تكن كافية لتأكيد وجود علاقة مستمرة بين الارتفاع والفرق الرأسي. وأشار سطح **IDW** إلى فروق أقل في القطاعين الغربي والشمالي الغربي، غير أن عدم انتظام توزيع النقاط وغياب التحقق المستقل حدّا من تفسير هذا النمط. وعليه، ينبغي استخدام ارتفاعات **AW3D30** غير المصححة بحذر في التطبيقات التي تتطلب دقة رأسية أعلى من مستوى الأداء المحلي المرصود.

الكلمات الدالة: ALOS AW3D30؛ الدقة الرأسية؛ التحقق باستخدام GNSS ؛ نموذج السطح الرقمي.

1. Introduction

Global digital elevation models provide essential topographic information for terrain analysis, environmental modelling, infrastructure planning, hydrological applications, and other geospatial investigations, particularly where detailed national elevation datasets or airborne LiDAR surveys are unavailable. Nevertheless, nominal grid spacing alone does not establish the vertical reliability or terrain-representation capability of a global elevation product. Differences in sensor technology, processing procedures, surface representation, and geographic conditions can produce substantial variations among global models, making local evaluation necessary before their use in applications with defined accuracy requirements [1].

The Advanced Land Observing Satellite World 3D 30 m (AW3D30) is a freely available global digital surface model (DSM) provided by the Japan Aerospace Exploration Agency (JAXA), with a spatial resolution of approximately 30 m and derived from optical stereo observations. Because it represents the visible surface, its elevations may include the effects of vegetation, buildings, and other above-ground features. Evaluations conducted across different terrain classes have shown that AW3D30 performance varies with slope, land cover, and local surface conditions [2]. The choice of global elevation model can also influence the representation of landform geometry and derived morphometric parameters, particularly where terrain morphology is complex [3].

Consequently, vertical accuracy values reported for one geographic environment cannot be transferred directly to another without independent verification. Comparative assessments in the South American Andes, for example, demonstrated that the relative performance of AW3D30 and other global elevation products changes among terrains and analytical settings [4]. For northeastern Libya, the magnitude, direction, and spatial variability of AW3D30 vertical differences remain insufficiently documented. It is therefore uncertain whether elevations within the area north of Al-Marj are centred around independent ground measurements or exhibit a consistent signed tendency. In regions where dense national elevation-reference datasets are limited, locally available GNSS observations provide a practical basis for assessing the suitability of global elevation products rather than relying solely on accuracy values obtained elsewhere [5].

The objective of this study is to quantify the vertical accuracy of AW3D30 using 23 GNSS checkpoints distributed north of Al-Marj, Libya. Elevations from both sources are compared within a common horizontal and vertical reference framework, and the resulting differences are evaluated using mean error, mean absolute error, root mean square error, and standard deviation. Their broad spatial variation

is additionally represented through exploratory inverse distance weighted interpolation. The study contributes a local estimate of the direction, magnitude, and dispersion of AW3D30 vertical differences in a coastal-to-inland environment for which published validation evidence is limited. The findings provide an initial basis for assessing the use of AW3D30 in applications whose vertical-accuracy requirements are compatible with its observed local performance.

2. Materials and Methods

The methodology was developed to assess the vertical accuracy of the AW3D30 DSM using GNSS checkpoints. It includes data preparation, elevation extraction, statistical accuracy assessment, and spatial analysis.

2.1 Methodological Workflow

The study followed a sequential GIS-based workflow, beginning with the delineation of the study area and the acquisition of the AW3D30 DSM and 23 GNSS checkpoints. Both datasets were prepared within a common horizontal and vertical reference framework, followed by DSM clipping, GNSS point-layer preparation, and extraction of the AW3D30 elevation corresponding to each checkpoint location. Point-wise vertical differences were then calculated and summarised using ME, MAE, RMSE, and SD. Finally, IDW interpolation was applied solely as an exploratory representation of the spatial variation in the observed differences. The complete methodological sequence is illustrated in Figure 1.

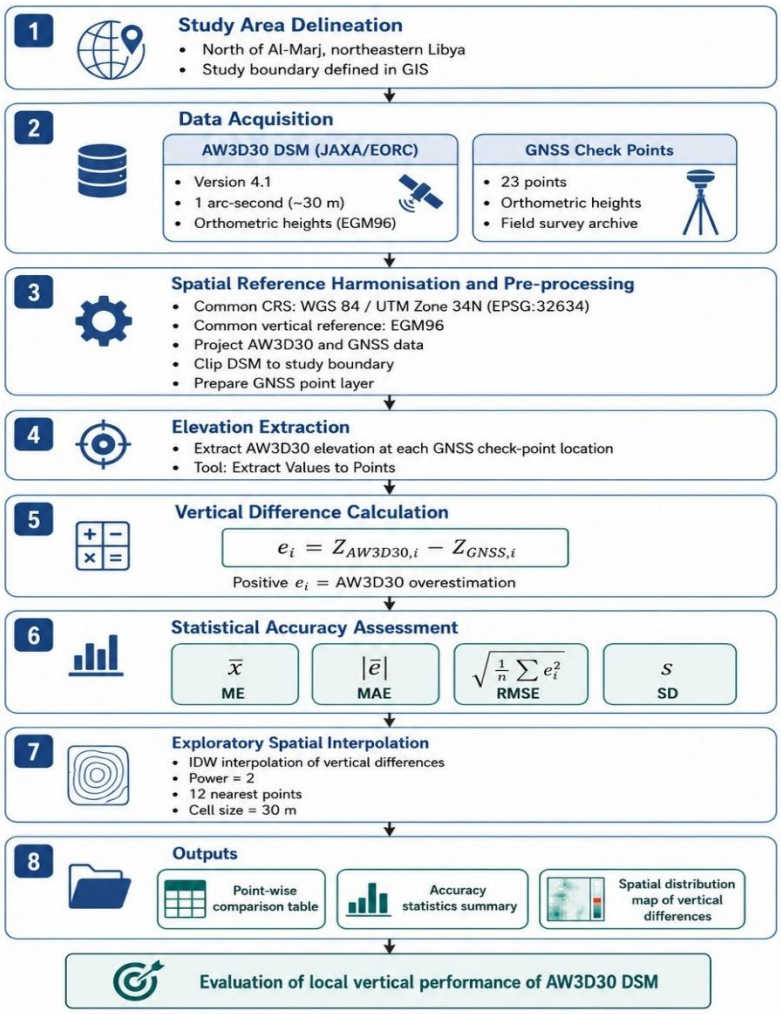

Figure 1. Workflow for AW3D30 vertical accuracy assessment using GNSS checkpoints.

2.2 Study Area

The study area is located north of Al-Marj in northeastern Libya, within the Al Jabal Al Akhdar region, and extends between the coastal locality of Tolmeitha and the inland area of Butraba. It was delineated in WGS 84 / UTM Zone 34N (EPSG:32634) by the following four vertices: (482,226.03 E, 3,613,292.70 N), (473,946.40 E, 3,609,738.45 N), (481,912.34 E, 3,599,305.23 N), and (488,537.55 E, 3,604,350.91 N). Based on these coordinates, the polygon covers approximately 102.89 km², equivalent to 10,289.16 ha. Its coordinate envelope spans about 14.59 km east–west and 13.99 km north–south. The location and boundary are shown in Figure 2.

Visual interpretation of the georeferenced Sentinel-2 images and the AW3D30 DSM indicates a transition from coastal lowlands in the north and north-west to more dissected inland terrain towards the south. Agricultural surfaces and valley features are also present within the boundary. The same polygon was used to clip the AW3D30 DSM, select the GNSS checkpoints, and define the spatial extent of the subsequent analyses.

2.3 Data Sources

Two primary datasets were used in the vertical accuracy assessment: the ALOS World 3D–30m digital surface model and an archive of 23 GNSS checkpoints. Only these datasets entered the elevation comparison. Their principal characteristics and analytical roles are summarised in Table 1. The AW3D30 raster and the point records were organised in ArcMap 10.8 before coordinate and vertical-reference harmonisation.

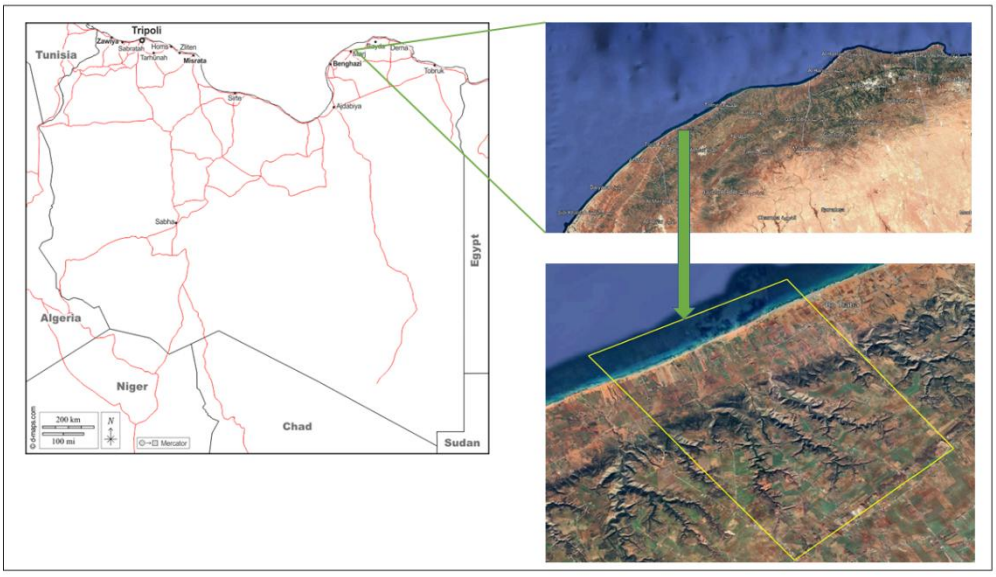

Figure 2. Location and boundary of the study area north of Al-Marj, north-eastern Libya

2.3.1 AW3D30 Digital Surface Model

The elevation surface evaluated in this study was the ALOS World 3D–30m digital surface model, commonly referred to as AW3D30. The product is distributed by the Earth Observation Research Center of the Japan Aerospace Exploration Agency. It was developed from the higher-resolution ALOS World 3D dataset, which was generated using stereo imagery acquired by the Panchromatic Remote-sensing Instrument for Stereo Mapping aboard the Advanced Land Observing Satellite between 2006 and 2011.

Table 1. Principal datasets used in the vertical accuracy assessment.

Dataset	Provider	Data structure	Main characteristics	Role in the assessment
AW3D30 DSM, Version 4.1	JAXA/EORC	GeoTIFF raster	One-arc-second grid; approximately 30 m; orthometric elevations referenced to EGM96	Elevation surface evaluated
GNSS checkpoint dataset	Bashir Jouda Engineering Works, Libya	Point records	23 points collected during 2019–2024; projected horizontal coordinates and orthometric heights	Ground dataset used for comparison

AW3D30 represents the visible land surface and may therefore include buildings, vegetation, and other above-ground objects. It is a digital surface model rather than a bare-earth digital terrain model. Version 4.1, released in April 2024 for global land areas outside Japan and Antarctica, was used for the present analysis. This release incorporated additional elevation sources for void filling and corrections to selected anomalous or incomplete areas. AW3D30 is distributed as one-degree-by-one-degree tiles. At the latitude of the study area, each tile contains a 3600 × 3600 grid with a nominal spacing of one arc-second, corresponding to approximately 30 m. The horizontal reference is WGS 84, and the elevation file is supplied in GeoTIFF format [6].

The product stores orthometric elevations in metres. These values were converted by JAXA from ellipsoidal heights defined in ITRF97 on the GRS80 ellipsoid using the EGM96 geoid model. Elevations are stored as integer values, and each cell contains a representative elevation for its pixel area. JAXA reports a target vertical accuracy of 5 m RMS for the product, although local performance may vary with terrain and land-cover conditions [7,8].

Each AW3D30 distribution package contains the principal DSM raster together with auxiliary files describing masks, source-image stacking, header information, quality information, and the source-scene list [6]. The DSM file was used as the numerical elevation input in this study. The auxiliary files were retained as product metadata and were not treated as independent elevation layers. The tile covering northern Al-Marj was downloaded from the official JAXA/EORC distribution portal. Its original spatial coverage and the position of the study boundary are shown in Figure 3 before clipping.

2.3.2 GNSS Checkpoint Dataset

The ground dataset consisted of 23 archived GNSS survey points supplied by Bashir Jouda Engineering Works, a licensed engineering and surveying office in Libya. The points had been observed during separate survey campaigns undertaken between 2019 and 2024 using a STONEX X10 GNSS receiver. The office supplied a point identifier, two projected horizontal-coordinate fields, and an orthometric height for each record. The elevations ranged from 1.06 to 312.11 m. These observations were treated as **GNSS checkpoints**, rather than ground control points, because they were used only to evaluate AW3D30 and did not contribute to the generation, adjustment, or correction of the DSM. Records were screened for completeness and spatial inclusion within the study boundary. The supplied coordinate and height fields are listed in Table 2.

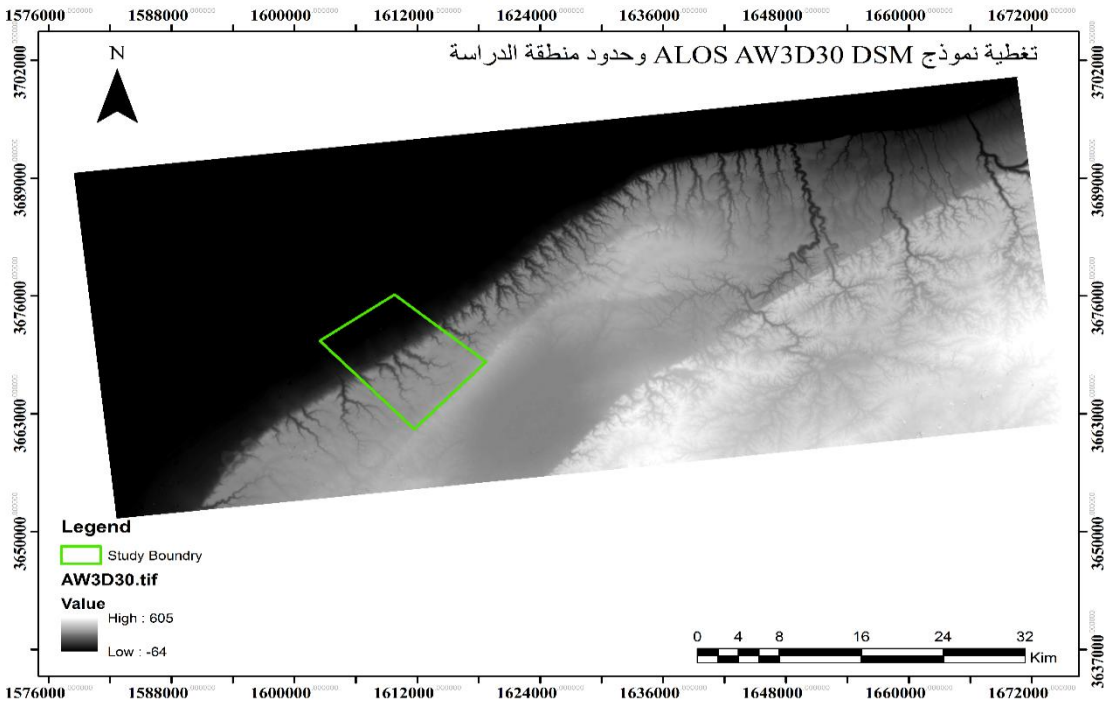

Figure 3. Original AW3D30 DSM coverage downloaded from JAXA/EORC and the boundary of the study area prior to raster clipping.

Table 2. Source coordinates and orthometric heights of the 23 GNSS checkpoints.

Point No.	Source X coordinate (m)	Source Y coordinate (m)	Orthometric height (m)
1	1,607,046.114	3,669,113.751	48.68
2	1,609,934.562	3,671,414.441	41.12
3	1,611,808.863	3,672,400.051	38.28
4	1,613,209.039	3,672,440.545	88.91
5	1,605,291.012	3,669,632.226	13.81
6	1,610,085.333	3,669,050.553	182.07
7	1,611,231.558	3,670,261.032	207.72
8	1,613,034.964	3,671,118.561	255.64
9	1,614,481.895	3,671,798.269	243.62
10	1,614,199.225	3,669,778.507	299.65
11	1,612,217.567	3,668,232.492	290.89
12	1,610,302.499	3,667,602.179	277.22
13	1,607,888.584	3,666,092.636	289.07
14	1,608,809.479	3,664,930.377	294.53
15	1,611,506.665	3,666,061.130	301.67
16	1,616,971.414	3,669,359.167	307.32
17	1,615,800.500	3,667,014.934	303.34
18	1,614,368.330	3,666,953.865	307.81
19	1,613,246.143	3,664,632.590	306.52
20	1,612,484.910	3,663,170.329	312.11
21	1,610,829.903	3,662,699.965	299.73
22	1,607,343.884	3,671,428.436	4.29
23	1,611,328.827	3,674,026.324	1.06

The observations originated from several survey campaigns rather than from a sampling network designed specifically for AW3D30 validation. Their spatial distribution was therefore non-uniform. No points were used to modify the AW3D30 raster. After coordinate and vertical-reference harmonisation,

the 23 records were converted to a GIS point layer and used as the locations at which AW3D30 elevations were extracted.

2.4 Spatial Reference Harmonisation and Data Pre-processing

All spatial processing was performed in ArcMap 10.8. The AW3D30 DSM and the GNSS checkpoint layer were stored and analysed in WGS 84 / UTM Zone 34N (EPSG:32634), which was retained as the common projected coordinate reference system throughout the analysis. The GNSS records were imported using the *Add XY Data* tool, and their documented coordinate system was defined during layer creation. The spatial references, layer extents, and point locations were subsequently verified to identify coordinate reversal, projection-assignment errors, or gross horizontal misalignment. Because the analytical layers were already referenced to the same projected coordinate system, no further horizontal coordinate transformation was applied.

The AW3D30 DSM was checked for spatial coverage, cell size, and valid elevation values. It was then clipped to the study boundary using the Extract by Mask tool. The DSM was retained at its existing nominal 30 m spatial resolution, and no additional reprojection, resampling, smoothing, terrain filtering, or elevation correction was applied during this stage. NoData cells remained undefined and were excluded from the subsequent point-based comparison.

Both datasets were expressed as orthometric heights referenced to the EGM96 geoid model. Standardising the vertical reference before extracting and comparing elevation values is necessary to prevent vertical-datum differences from being incorporated into the estimated DEM errors [9]. The geoid provides the reference surface required for deriving orthometric heights from satellite-positioning observations, and compatibility between the reference and checkpoint height systems is essential for reliable vertical comparison [10]. The GNSS observations were processed using EGM96; therefore, the comparison was conducted within a common vertical reference without applying any preliminary vertical offset, local height adjustment, or bias correction.

AW3D30 elevations were assigned to the 23 GNSS checkpoint locations using the Extract Values to Points tool. Interpolation at the point locations was disabled, so each check point received the value of the raster cell containing its location. No check point coincided with a NoData cell. The resulting matched dataset retained the GNSS orthometric heights and the corresponding integer AW3D30 elevations used in the vertical-accuracy calculations. This point-based matching approach is consistent with recent frameworks for assessing global DEM accuracy using independent reference points [11].

2.5 Computation of Vertical Differences and Accuracy Metrics

A paired elevation record was created for each of the 23 GNSS checkpoints, containing the projected coordinates, the extracted AW3D30 elevation, and the corresponding GNSS orthometric height. The point-wise vertical difference was calculated as:

$$e_i = Z_{\mathrm{AW3D30},i} - Z_{\mathrm{GNSS},i} \tag{1}$$

where e_i is the vertical difference at the checkpoint i, $Z_{\mathrm{AW3D30},i}$ is the elevation extracted from the DSM, and $Z_{\mathrm{GNSS},i}$ is the GNSS orthometric height. A positive value indicates that AW3D30 overestimates the ground elevation, whereas a negative value indicates underestimation. The complete paired dataset, including the coordinates and calculated vertical differences, is presented in Table 3.

Four statistical measures were calculated to describe the systematic tendency, absolute magnitude, overall accuracy, and dispersion of the vertical differences. The mean error was computed as:

$$\mathrm{ME} = \frac{1}{n}\sum_{i=1}^{n} e_i \tag{2}$$

The mean absolute error was calculated as:

$$\mathrm{MAE} = \frac{1}{n}\sum_{i=1}^{n} |e_i| \tag{3}$$

The root mean square error was calculated as:

$$\mathrm{RMSE} = \sqrt{\frac{1}{n}\sum_{i=1}^{n} {e_i}^2} \tag{4}$$

The sample standard deviation of the vertical differences was determined as:

$$\mathrm{SD} = \sqrt{\frac{\sum_{i=1}^{n}(e_i - \overline{e})^2}{n-1}} \tag{5}$$

where $n = 23$, $\overline{e}$ is the mean vertical difference, and i represents the checkpoint index. ME describes the direction and magnitude of systematic vertical bias. MAE expresses the average absolute discrepancy without considering its sign, while RMSE gives greater weight to larger differences. SD measures the variability of the individual differences around the mean error.

2.6 Exploratory Spatial Interpolation of Vertical Differences Using IDW

The point-wise vertical differences calculated at the 23 GNSS checkpoints were used as the input variable for spatial interpolation in ArcMap 10.8. An inverse distance weighted (IDW) surface was generated to examine the broad spatial variation in the magnitude of the AW3D30–GNSS differences between the sampled locations. IDW estimates an unknown value as a distance-weighted average of surrounding observations, assigning greater influence to nearby points than to more distant points:

$$\hat{e}(x_0) = \frac{\sum_{i=1}^{m} e_i \, {d_{i0}}^{-p}}{\sum_{i=1}^{m} {d_{i0}}^{-p}} \tag{6}$$

where $\hat{e}(x_0)$ is the estimated vertical difference at an unsampled location x_0, e_i is the observed vertical difference at the check point i, d_{i0} is the horizontal distance between the check point i and the estimated location, m is the number of neighbouring points included in the estimation, and p is the distance-decay power.

The interpolation was performed using the IDW tool in the Spatial Analyst extension. A power value of $p = 2$ was adopted, producing inverse-square distance weighting. A variable search radius containing the 12 nearest checkpoints was used for each estimated cell. The output cell size was set to a nominal 30 m, consistent with the processed AW3D30 raster, which was also used as the snap-raster reference. The interpolation extent was restricted to the study boundary, and the resulting surface was clipped using the same boundary polygon. No barriers or directional weighting were applied.

The continuous raster was subsequently divided into graduated classes for cartographic presentation. This classification affected only the visual display and did not alter the underlying interpolated values. The IDW surface was used as an exploratory representation of the spatial arrangement of the observed differences and did not contribute to the calculation of ME, MAE, RMSE, or SD.

Because the 23 checkpoints were unevenly distributed and no independent validation or leave-one-out cross-validation was performed, the interpolated surface was not treated as a validated prediction of AW3D30 accuracy at unsampled locations. Its interpretation was limited to illustrating broad spatial variation under the specified distance-weighting assumptions.

3. Results and Discussion

This section presents the vertical accuracy assessment of the AW3D30 DSM using independent GNSS reference points. The results and statistical analysis are discussed in the following subsections.

3.1 Spatial Distribution of GNSS Checkpoints and AW3D30 Elevations

Figure 4 presents the clipped AW3D30 digital surface model and the locations of the 23 GNSS checkpoints used for vertical accuracy assessment. AW3D30 elevations within the study boundary ranged from approximately −2 to 376 m and showed a general increase from the northern and north-western coastal sector towards the inland and southern parts of the study area. The minimum value of approximately −2 m occurred within the coastal margin of the raster and did not coincide with a GNSS check point. It is therefore reported as an extreme value within the AW3D30 domain rather than interpreted as an independently verified below-sea-level ground elevation.

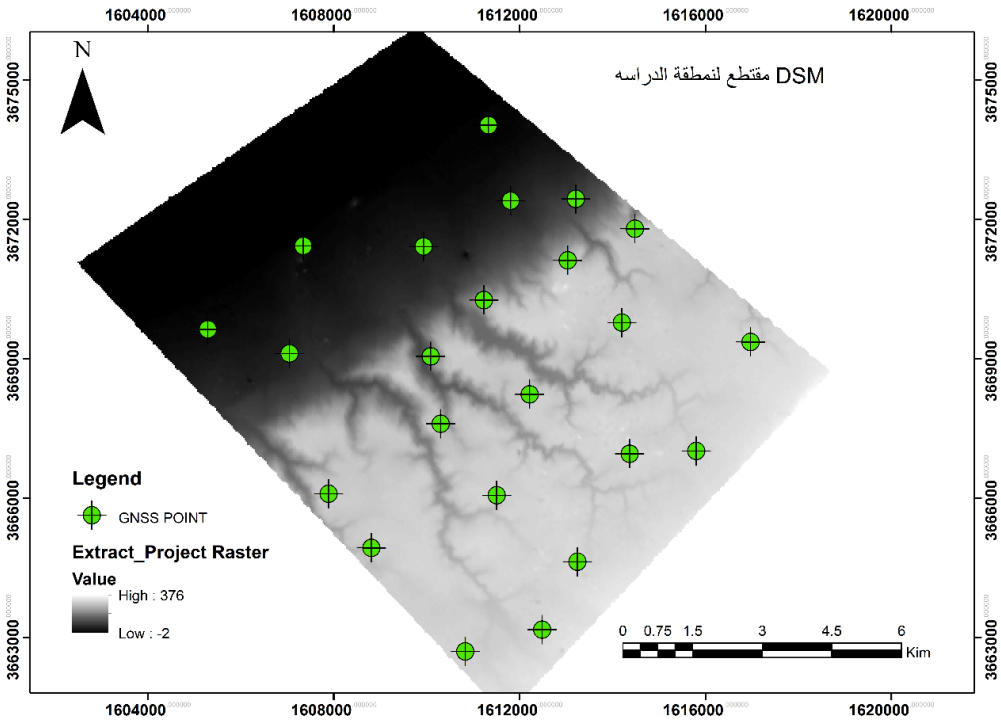

Figure 4. Spatial distribution of the 23 GNSS checkpoints over the clipped AW3D30 digital surface model of the study area.

Spatial distribution of the 23 GNSS checkpoints superimposed on the clipped AW3D30 digital surface model. Elevations are expressed in metres relative to the common orthometric-height reference described in Section 2.3. The GNSS elevations ranged from 1.06 to 312.11 m, giving an observed range of 311.05 m. This corresponds to approximately 82% of the total elevation range represented by the AW3D30 DSM within the study boundary. This percentage describes only the numerical coverage of the elevation range and should not be interpreted as equivalent spatial coverage of the study area. The median GNSS elevation was 277.22 m, which lies close to the upper end of the observed GNSS range and indicates that the checkpoint dataset was weighted towards higher elevations. The spacing of the

points was also non-uniform; consequently, the dataset represents the conditions at the sampled locations rather than a regular or spatially exhaustive validation of the entire AW3D30 DSM.

A visual comparison suggests that the GNSS elevations follow the broad increase in elevation represented by the AW3D30 DSM from the coastal sector towards the inland terrain. This observation is qualitative and does not establish vertical agreement between the two datasets. The direction and magnitude of the elevation differences were therefore evaluated quantitatively using point-wise AW3D30–GNSS differences in the following subsection.

3.2 Comparison between AW3D30 and GNSS Elevations

Table 3 compares the AW3D30 elevations extracted at the 23 GNSS checkpoint locations with the corresponding GNSS measurements. The pointwise difference was defined as AW3D30 minus GNSS elevation. AW3D30 produced higher values at every checkpoint, with differences ranging from 2.19 m at Point 5 to 9.78 m at Point 12.16 of the 23 differences were at least 7 m, whereas only 7 were below this value. The absence of negative differences indicates a consistent positive offset rather than errors distributed randomly around zero. The magnitude of this offset is examined statistically in Section 3.3.

The differences also varied across the sampled elevation range. At the seven checkpoints with GNSS elevations below 100 m, the differences ranged from 2.19 to 5.32 m. In contrast, the remaining 16 points, all located above 180 m, showed differences between 7.19 and 9.78 m. This separation suggests that larger discrepancies occurred at the higher sampled elevations. It should not, however, be interpreted as an elevation-dependent error relationship without further analysis. Elevation, geographic location, terrain conditions, and surface cover were not evaluated independently, and the checkpoint dataset contained no observations between 88.91 and 182.07 m. The result therefore identifies a pattern within the available sample but does not establish its underlying cause.

Table 3. AW3D30 and GNSS elevations and their point-wise vertical differences

Point No.	AW3D30 elevation (m)	GNSS elevation (m)	Vertical difference, AW3D30 − GNSS (m)
1	54.00	48.68	5.32
2	44.00	41.12	2.88
3	42.00	38.28	3.72
4	94.00	88.91	5.09
5	16.00	13.81	2.19
6	190.00	182.07	7.93
7	215.00	207.72	7.28
8	265.00	255.64	9.36
9	251.00	243.62	7.38
10	308.00	299.65	8.35
11	299.00	290.89	8.11
12	287.00	277.22	9.78
13	298.00	289.07	8.93
14	304.00	294.53	9.47
15	310.00	301.67	8.33
16	315.00	307.32	7.68
17	312.00	303.34	8.66
18	315.00	307.81	7.19
19	316.00	306.52	9.48
20	321.00	312.11	8.89
21	309.00	299.73	9.27
22	7.00	4.29	2.71
23	5.00	1.06	3.94

3.3 Statistical Assessment of Vertical Accuracy

Table 4 summarises the vertical accuracy statistics derived from the 23 AW3D30–GNSS elevation differences. The mean error and the mean absolute error were 7.04 m. Their identical values were reflected by uniformly positive differences observed at all checkpoints, indicating that AW3D30 consistently produced elevations higher than the corresponding GNSS measurements within the sampled locations.

Table 4. Summary statistics of the AW3D30–GNSS vertical differences at the 23 checkpoints.

Accuracy metric	Symbol	Value (m)
Mean error	ME	7.04
Mean absolute error	MAE	7.04
Root mean square error	RMSE	7.44
Sample standard deviation	SD	2.45

The RMSE was 7.44 m, exceeding the MAE by only 0.40 m. This limited difference indicates that the larger discrepancies had only a moderate additional influence on the overall error magnitude and that the results were not characterised by isolated extreme values. The sample standard deviation of 2.45 m shows that the positive differences varied between checkpoints, although this variability remained smaller than the mean offset itself.

Taken together, the statistics show that the observed vertical discrepancy was dominated by a persistent positive offset, accompanied by a lower level of point-to-point variation. AW3D30 therefore did not fluctuate around the GNSS measurements; it overestimated elevation at every sampled location. The variation identified in Section 3.2 also indicates that the magnitude of this overestimation was not constant across the dataset, which limits the usefulness of interpreting the mean difference as a uniform correction for the entire study area.

3.4 IDW Representation of the Spatial Variation in Vertical Differences

The point-wise AW3D30 and GNSS vertical differences ranged from 2.19 to 9.78 m, giving an observed spread of 7.59 m across the 23 checkpoints. All differences were positive; the spatial variation concerned the magnitude of AW3D30 overestimation rather than a change in the direction of the discrepancy. To visualise the broad spatial arrangement of the observed values, an IDW-interpolated surface was produced, as shown in Figure 5.

The IDW surface assigns lower interpolated differences mainly to the western and north-western sectors, where nearby checkpoints recorded values between approximately 2.19 and 5.32 m. Higher interpolated values occur across parts of the central, southern, and south-eastern sectors and are influenced by checkpoints with differences reaching 9.78 m. The surface therefore extends the observed point-wise differences spatially according to the selected IDW weighting scheme; it does not provide independent confirmation of the apparent spatial arrangement.

The interpolated zones should be interpreted cautiously, particularly in peripheral and sparsely sampled areas. Their extent and boundaries depend on the locations and values of the 23 non-uniformly distributed checkpoints, and no independent observations were available to evaluate prediction accuracy between them. The map consequently provides an exploratory representation of broad spatial variation, rather than evidence of a verified fine-scale error pattern. It also does not establish whether the variation was associated with elevation, terrain, surface cover, or another spatial factor. The observed variability does not preclude the possible usefulness of a mean-bias correction, but such a correction would not remove the remaining location-specific differences and should be assessed quantitatively before application to the entire AW3D30 DSM.

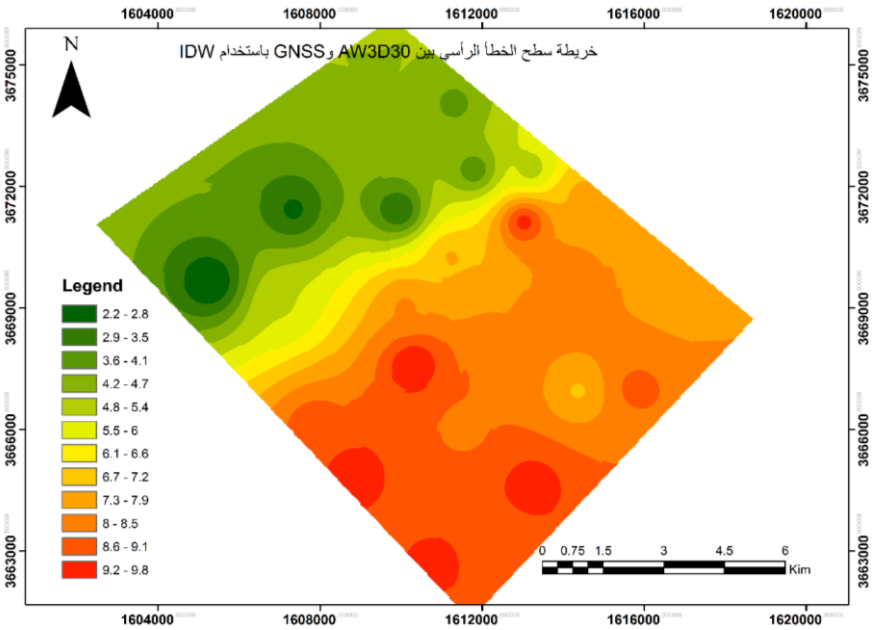

Figure 5. Exploratory IDW-interpolated surface of the AW3D30–GNSS vertical differences derived from 23 GNSS checkpoints.

3.5 Discussion

The RMSE obtained in this study was 7.44 m, while the mean AW3D30–GNSS difference was 7.04 m. These values are broadly consistent with the range reported in previous site-specific assessments, although direct comparison requires caution. Santillan and Makinano-Santillan reported an RMSE of 5.68 m in northeastern Mindanao, while González-Moradas and Viveen obtained 6.246 m across four regions in Peru [12,13]. Nikolakopoulos reported an overall RMSE of 7.67 m in Greece, but the error varied markedly between low-relief and more complex terrain [14]. By contrast, Caglar et al. obtained 1.78 m using a runway-based method applied to relatively flat and unobstructed surfaces [15]. The positive mean difference observed here also falls within the 2.99–7.75 m range reported by Uuemaa et al. across four study regions [16]. These results indicate that AW3D30 accuracy is strongly dependent on the evaluation setting. Differences in terrain, land cover, reference data, sampling density, matching procedures, and vertical-reference treatment prevent the reported statistics from being treated as directly interchangeable.

The consistently positive differences may reflect several effects acting together. AW3D30 is a digital surface model, whereas each GNSS check point represents a discrete surveyed location. Vegetation, buildings, and other above-ground features within a 30 m raster cell may therefore increase the AW3D30 elevation relative to the ground measurement. The comparison also involves different spatial supports: GNSS represents a very small ground position, while AW3D30 represents an area of approximately 30 × 30 m. In sloping or heterogeneous terrain, horizontal co-registration differences and the location of the GNSS point within the raster cell may appear as additional vertical discrepancies. Temporal mismatch is another possible source. The GNSS observations were collected between 2019 and 2024, whereas the ALOS imagery used to generate AW3D30 predates those surveys. Any local modification of roads, fields, or built surfaces during the intervening period may contribute to the measured differences. These effects were not isolated individually in the present study, but their relevance is consistent with the influence of morphology, roughness, slope, and land cover reported by Trevisani et al. [17].

A clear descriptive separation was observed across the sampled elevation range. The seven checkpoints below 100 m had differences of 2.19–5.32 m, whereas the 16 points above 180 m had differences of 7.19–9.78 m. This pattern does not establish a continuous relationship between elevation and vertical difference. The dataset contains no observations between 88.91 and 182.07 m, and the apparent elevation effect may be confounded with location, slope, terrain form, or surface cover. González-Moradas and Viveen did not find a consistent relationship with absolute elevation, but they reported larger residuals on slopes exceeding 15° [13]. Uuemaa et al. likewise identified slope as a more consistent influence on DEM accuracy than aspect [16]. Since slope and land-cover effects were not analysed separately here, the cause of the observed separation cannot be determined from the available sample.

The IDW map should be regarded as a descriptive extension of the 23 observed differences rather than as an independently validated error surface. The interpolated values reproduce the spatial arrangement of the checkpoint data according to the selected distance-weighting assumptions. No independent validation or leave-one-out cross-validation was performed; therefore, the mapped zones should not be treated as validated predictions at unsampled locations. From an applied perspective, the measured RMSE limits the direct use of uncorrected AW3D30 elevations in applications whose specified vertical tolerance is substantially below this value. A mean-bias correction could reduce the dominant positive component, but it would not remove the remaining location-specific variation. Fragozo Arevalo et al. demonstrated that GNSS- and land-cover-based correction can improve global DEM elevations, but their study used a much larger dataset and separate calibration and validation subsets in a low-gradient floodplain [18]. The present sample is too small and unevenly distributed to support direct adoption of the same correction framework.

The principal limitations are the restricted number and non-uniform distribution of the GNSS checkpoints, their concentration at higher elevations, the unsampled intermediate elevation range, and the absence of stratified analysis by slope, land cover, or terrain roughness. The IDW surface was not validated, and the effects of temporal change, horizontal co-registration, and raster-cell support were not quantified. Within these constraints, the study provides a local estimate of the magnitude and variability of AW3D30–GNSS differences north of Al-Marj. It does not represent a spatially exhaustive validation of AW3D30 across the wider region.

4. Conclusions

This study assessed the vertical accuracy of the AW3D30 digital surface model north of Al-Marj using 23 GNSS checkpoints, with both datasets referenced to a common horizontal and vertical framework. AW3D30 produced higher elevations at every sampled location, with vertical differences ranging from 2.19 to 9.78 m. The mean error and mean absolute error were both 7.04 m, while the RMSE and sample standard deviation were 7.44 and 2.45 m, respectively. These findings show consistently positive vertical differences accompanied by measurable point-to-point variability. Consequently, a single uniform correction should not be applied across the study area without further validation. The exploratory IDW surface indicated broad spatial variation, although its interpretation is limited by the uneven point distribution and the absence of independent validation. Uncorrected AW3D30 elevations should therefore be used cautiously in applications requiring vertical accuracy better than the observed local performance. A further limitation is the relatively small number of GNSS checkpoints (23 points), which resulted in an underrepresented elevation interval between 88.91 m and 182.07 m. Future work should use a larger and more evenly distributed GNSS dataset, include intermediate and higher elevation ranges, particularly across Al Jabal Al Akhdar, examine terrain and land-cover effects, and independently evaluate any proposed correction model.

REFERENCES

[1] Guth, P.L.; Trevisani, S.; Grohmann, C.H.; Lindsay, J.; Gesch, D.B.; Hawker, L.; Bielski, C. Ranking of 10 global one-arc-second DEMs reveals limitations in terrain morphology representation. Remote Sens., 2024, 16(17), 3273. doi:10.3390/rs16173273.

[2] Li, H.; Zhao, J.; Yan, B.; Yue, L.; Wang, L. Global DEMs vary from one to another: An evaluation of newly released Copernicus, NASA and AW3D30 DEM on selected terrains of China using ICESat-2 altimetry data. Int. J. Digit. Earth, 2022, 15(1), 1149–1168. doi:10.1080/17538947.2022.2094002.

[3] Zhang, R.; Kereszturi, G.; Brenna, M.; Ahn, U.S. Sensitivity assessment of morphometric parameters of monogenetic volcanic landforms with global free DEMs. Geomorphology, 2022, 415, 108408. doi: 10.1016/j.geomorph.2022.108408.

[4] González-Moradas, M. del R.; Viveen, W.; Vidal-Villalobos, R.A.; Villegas-Lanza, J.C. A performance comparison of SRTM v. 3.0, AW3D30, ASTER GDEM3, Copernicus and TanDEM-X for tectonogeomorphic analysis in the South American Andes. CATENA, 2023, 228, 107160. doi: 10.1016/j.catena.2023.107160.

[5] Nandam, V.; Patel, P.L. A framework to assess suitability of global digital elevation models for hydrodynamic modelling in data-scarce regions. J. Hydrol., 2024, 630, 130654. doi: 10.1016/j.jhydrol.2024.130654.

[6] Grigoriadis, V.N.; Andritsanos, V.D.; Natsiopoulos, D.A. Validation of recent DSM/DEM/DBMs in test areas in Greece using spirit leveling, GNSS, gravity and echo sounding measurements. ISPRS Int. J. Geo-Inf., 2023, 12(3), 99. doi:10.3390/ijgi12030099.

[7] Meadows, M.; Jones, S.; Reinke, K. Vertical accuracy assessment of freely available global DEMs (FABDEM, Copernicus DEM, NASADEM, AW3D30 and SRTM) in flood-prone environments. Int. J. Digit. Earth, 2024, 17(1). doi:10.1080/17538947.2024.2308734.

[8] Huang, J.; Yang, Y.; Yu, Y.; Zhang, Y. Vertical accuracy of open-source remote sensing data (AW3D30, TanDEM-X, ATLAS) for understory terrain estimation. Geocarto Int., 2024, 39(1). doi:10.1080/10106049.2024.2356855.

[9] Xu, W.; Li, J.; Peng, D.; Yin, H.; Jiang, J.; Xia, H.; Wen, D. Vertical accuracy assessment and improvement of five high-resolution open-source digital elevation models using ICESat-2 data and random forest: Case study on Chongqing, China. Remote Sens., 2024, 16(11), 1903. doi:10.3390/rs16111903.

[10] Abbak, R.A.; Goyal, R.; Ustun, A. A user-friendly software package for modelling gravimetric geoid by the classical Stokes–Helmert method. Earth Sci. Inform., 2024, 17, 3811–3824. doi:10.1007/s12145-024-01328-0.

[11] Shahabi, E.; Jafari, M.; Taheri Dehkordi, A. A new framework for vertical accuracy assessment and spatial error mapping of global digital elevation models using ICESat-2. J. Geovis. Spat. Anal., 2026, 10, Article 2. doi:10.1007/s41651-025-00245-0.

[12] Santillan, J.R.; Makinano-Santillan, M. Vertical accuracy assessment of 30-m resolution ALOS, ASTER, and SRTM global DEMs over northeastern Mindanao, Philippines. Int. Arch. Photogramm. Remote Sens. Spatial Inf. Sci., 2016, XLI-B4, 149–156. doi:10.5194/isprs-archives-XLI-B4-149-2016.

[13] González-Moradas, M.R.; Viveen, W. Evaluation of ASTER GDEM2, SRTMv3.0, ALOS AW3D30 and TanDEM-X DEMs for the Peruvian Andes against highly accurate GNSS ground control points and geomorphological-hydrological metrics. Remote Sens. Environ., 2020, 237, 111509. doi:10.1016/j.rse.2019.111509.

[14] Nikolakopoulos, K.G. Accuracy assessment of ALOS AW3D30 DSM and comparison to ALOS PRISM DSM created with classical photogrammetric techniques. Eur. J. Remote Sens., 2020, 53(sup2), 39–52. doi:10.1080/22797254.2020.1774424.

[15] Caglar, B.; Becek, K.; Mekik, C.; Ozendi, M. On the vertical accuracy of the ALOS World 3D-30m digital elevation model. Remote Sens. Lett., 2018, 9(6), 607–615. doi:10.1080/2150704X.2018.1453174.

[16] Uuemaa, E.; Ahi, S.; Montibeller, B.; Muru, M.; Kmoch, A. Vertical accuracy of freely available global digital elevation models: ASTER, AW3D30, MERIT, TanDEM-X, SRTM, and NASADEM. Remote Sens., 2020, 12(21), 3482. doi:10.3390/rs12213482.

[17] Trevisani, S.; Skrypitsyna, T.N.; Florinsky, I.V. Global digital elevation models for terrain morphology analysis in mountain environments: Insights on Copernicus GLO-30 and ALOS AW3D30 for a large Alpine area. Environ. Earth Sci., 2023, 82, 198. doi:10.1007/s12665-023-10882-7.

[18] Fragozo Arevalo, J.M.; Escobar-Vargas, J.; Escobar Villanueva, J.R. Local altimetric correction of global DEMs in data-scarce floodplains: A practical GNSS-based approach. ISPRS Int. J. Geo-Inf., 2025, 14(12), 498. doi:10.3390/ijgi14120498.